Received: 28 January 2020 | Revised: 15 April 2020 | Accepted: 16 April 2020

DOI: 10.1002/ett.3985

SPECIAL ISSUE ARTICLE

WILEY

A novel approach for multimodality medical image fusion over secure environment

Pardeep Kumar[1] | **Manoj Diwakar**[2]

[1]CSE Department, Jaypee University of Information Technology, Solan, India

[2]CSE Department, Graphic Era Deemed to be University, Dehradun, India

Correspondence
Manoj Diwakar, CSE Department, Graphic Era Deemed to be University, Dehradun, Uttarakhand, India.
Email:manoj.diwakar@gmail.com

Summary

An emerging trend to deal with the issue of multimodality medical image fusion over the secure communication environment is required. Hence, this paper presents a human visual fusion algorithm for medical images such as computed tomography and magnetic resonance imaging which is based on the nonsubsampled shearlet transform (NSST) over the secure environment. Initially, the images are decayed through NSST into low and detailed highlights. The neighborhood aggregate of correlation-based movement measures is proposed to intertwine the low frequency and sum-modified-Laplacian-based fusion is utilized on detail subbands of NSST. After getting a fused image, a method noise thresholding approach is utilized to improve the accuracy of the proposed method. As a result, more accurate fused images is received. To measure the proposed method accuracy, the results of the fused images are also tested over the secure environment where encrypted/decrypted fused images are obtained using the random generator method. These decrypted fused images are also analyzed with original fused images with the proposed method as well as existing methods. From result analysis, it is observed that the proposed technique is better in holding a bone, calcification, cerebrospinal liquid, edema, and tumor subtleties of the source images and is more accurate than other existing fusion methods.

KEYWORDS

mutual information, neural network, parametric correlation, Shearlet domain

1 | INTRODUCTION

The interest for clinical image translation benefits in radiology is growing quickly everywhere throughout the world. This has featured the need of medical experts to resolve the medical-related issues for diagnosis purpose. Due to limited medical experts in the local areas, the issue of medical services can be overwhelmed by using strong communication to draw on the mastery of remotely found radiologists. The procedure where by medical images are moved to long distance areas with the end goal of understanding and analysis is characterized as teleradiology.[1,2] The role of medical image processing in telecommunications includes the securing and transmission of images from long distances. Numerous investigations in image processing such as image transformation-based malware classification,[3] secured medical image watermarking,[4,5] image deblurring,[6] etc., shows their latent capacity and the expectation made among the telecommunications network. In medical science, each development revolves around different organs/tissues and gives huge information regarding each

like the computed tomography (CT) imaging perceives thick structures like bones and it is more sensitive than magnetic resonance (MR) imaging in the investigation of breaks. MR imaging gives information related to soft issues to reflect absorption information of a peak, progresses like positron emission tomography (PET) and single-photon emission CT (SPECT), which holds an uncommon motivating force in vascular infirmity assurance and tumor acknowledgment. During the last few decades, medical image fusion has gained much attention to solve medical issues. The main application of this field is to extract the clinical information (medical imaging, treatment planning and to assist in surgical procedures) from different sensors which are generally may not be visible in the images. The few biomedical sensors such as X-ray, ultrasound, MR imaging, CT, and PET give the medical information by reflecting through the images of human body organs and cells are used in biomedical imaging.[7]

Generally, neurologists prefer bone and parenchymal details inside the medical images for the number of diagnosis tasks such as injury outline, PC-assisted neurosurgery, and radiation treatment.[8] There is no such low-cost medical tool that can provide complete medical details in a single image. Each medical modality has its own merits and limitations to get the medical details.[9] Hence, the image fusion approach can provide more informatics medical images by combining two or more than two medical images such as by combining CT and MRI images. The use of various imaging systems has increased the workload of human observers.[10] Due to numerous imaging systems, images like multifocus or multisensor of the same scene may have different information. The images may get blurred or degraded due to the varying image capturing conditions or camera calibration thus, they may not provide the whole information of the scene in the single image.[11] The images having less information may not provide appropriate information about the scene. For instance, medical images must be sharper for the diagnosis purpose. In some cases, we cannot easily identify the objects in images due to their low contrast. Due to the aforementioned conditions, it is quite difficult for a human operator to merge the reliable visual information by viewing and analyzing multiple images separately.[12] Hence, a fusion system is required which can provide a single fused image by merging the relevant information present in the images of the same scene obtained from the same or different capturing conditions. The obtained fused image is more informative with a better visual appearance than either of the single-source images. Image fusion provides better interpretation of the scene, accurate information, enhanced resolution, and robustness at low cost. Therefore, there is a need to develop novel and improved image fusion techniques to produce a more informative fused image for multifocus and multisensor images, which are useful for better interpretation of the scene. Generally, the quality of the fused image depends on the application requirements. In many applications, the perception and interpretation of a fused image play an important role in human observer. Consequently, another way to assess the quality of the fused image is its quantitative analysis. The qualitative analysis of the fused images is performed correctly but it is not sufficient due to the inconvenience and time consumption. Therefore, quantitative analysis can accurately measure the performance of the images.[13]

Transform domain-based multimodality image fusion is one of the popular ways where images are decomposed and fused. After getting success on discrete wavelet transform- (DWT) based multimodality image fusion, various transforms are also used such as curvelet-based image fusion, nonsubsampled contourlet transform- (NSCT) based image fusion and nonsubsampled shearlet transform- (NSST) based image fusion. Each transform has some merits and demerits such as DWT have limited direction as well as there is shift-invariance problem. The edges are also not effectively preserved in the DWT domain. Curvelets are an improvement to wavelets as far as a superior portrayal of bent information. In any case, these cannot be developed in the digital domain legitimately. Curvelet transform provides sharp and smooth curve edges. Further improvement in the multiresolution analysis is gotten utilizing contourlets and its other adaptation called NSCT.[14] In any case, contourlets have higher computational expense. An improvement to computational expense is brought by NSST which gives fusion results like NSCT. NSCT also provides sharp and smooth edges which can help to provide more accurate fused images.[15] NSST transform is also very popular in multimodality image fusion. NSST helps to avoid shift-invariance problem.[16] By using NSST, more features can be extracted by increasing multiple directions and multimodality image fusion operation can be performed.[17]

Over the previous years, many developers[18-22] have applied their fusion ways to deal with various kinds of multimodal images. The developers have utilized average and maximum selection rules with complex wavelet transform. A guided channel-based methodology with wavelet transform is shown by References 23,24. In Reference 25, an adaptive sparse representation- (SR) based multimodal image fusion method is utilized for fusion. Further, this plan has an extremely high computational multifaceted nature. Convolutional neural networks are also used for image fusion.[26-28] Ming Yin et al[29] proposed a parameter-adaptive PCNN (PA-PCNN) model which entwines high-frequency coefficients with the PCNN parameters which are resolved dependent on input bands, which further can vanquish the difficulty of setting free parameters in the PCNN models. Ming Yin et al, moreover, showed a novel low-frequency fusion method that keeps an

eye on two basic factors in therapeutic image fusion, to be explicit, essentialness preservation and detail extraction. These methodologies were driven on different sorts of helpful image fusion procedures to check its suitability.[30-32]

With the motivation of higher feature extraction by using NSST[33-35] and utilized that features for multimodality medical image fusion,[36-39] a new methodology is performed and also analyzed in secure environment.[17] The concept of method noise thresholding is generally utilized in medical image denoising which is used to improve the accuracy of the results. In this paper, method noise thresholding[19] is utilized in multimodality image fusion. Before this, method noise thresholding is never utilized with multimodality image fusion in the NSST domain. The objective of this paper is to develop the new and improved image fusion algorithms to extract the maximum image information and brief analysis of fused images over the secure environment. To increase the applicability of image fusion, the concentration is on developing the image fusion techniques which can give more information along with better visual quality. To evaluate the performance of fused images in terms of quantitative analysis, various types of quality measurement metrics have also been used. The layout of the remainder of the paper is given as follows: Section 2 gives a brief discussion on the concepts of shearlet transforms and the sum modified Laplacian method. Section 3 illustrates the point-by-point procedure of the proposed fusion method. Section 4 contains the visual and quantitative outcomes, discussions and examination of the created method with different strategies. Section 5 depicts the conclusions.

2 | PRELIMINARIES

In this section, the brief concepts of NSST and SML are described which is further used in the proposed fusion process.

2.1 | NONSUBSAMPLED SHEARLET TRANSFORM

Shearlet[29] is proved to be advantageous over other methods by capturing features of images in diverse directions and gives an optimal representation of the targeted image. Shearlet transform (ST) is better than the contourlet transform as there are multiple directions in shearlet. Also, the inverse shearlet transform requires a collection of shearing filters which increases its computational efficiency. One of the disadvantages of ST is that it causes a lack of shift uniformity (as it is important to prevent undesirable Gibbs phenomenon).To resolve this issue, NSST has been introduced which is a nonsubsampled version of shearlet transform and is based on pyramid filters, NSPFs (nonsubsampled pyramid filters) and filter banks, SFBs (shearlet filter banks).[24] It was used to get the multiscale decomposition of an image. If a decomposition method is applied for L levels, then subbands are obtained which are $L+1$ in number and include L number of bands of high-frequency and the band of low-frequency. To reconstruct the original image, inverse NSST is used which completes the process in two steps. Firstly the nonsubsampled pyramid is obtained using SFBs and then the resultant image is reconstructed by the obtained nonsubsampled pyramid using the reconstruction filters. NSST method is considered as an effective method of the fusion of images due to its properties like multiscale, multidirection, and shift-invariance. The shearlet transform depends on three variables, that is, the scale a, the orientation b, and the location c. Each $f \in L^2(R^2)$ can be recovered by:

$$f = \int_{R^2} \int_{-\infty}^{+\infty} \int_{0}^{+\infty} < f, \Psi_{a,b,c} > \Psi_{a,b,c} \frac{dp}{p^3} dqdt. \tag{1}$$

With the consideration, $a=2^{-2J}$, $b=-L$ with J, $c=K \in Z^2$ and $L \in Z$ the discrete shearlet transform expressed as:

$$\Psi_{a,b,c} = |detA_0|^{\frac{J}{2}} \Psi(B_0^L A_0^L x - K), \tag{2}$$

where $A_0 = \begin{pmatrix} 4 & 0 \\ 0 & 2 \end{pmatrix}$ and $B_0 = \begin{pmatrix} 1 & 1 \\ 0 & 1 \end{pmatrix}$

For each $f \in L^2(R^2)$, the characteristic Ψ can be expressed as below:

$$f = \sum_{J,L \in Z, K \in Z^2} < f, \psi_{J,L,K} > \psi_{J,L,K}. \tag{3}$$

2.2 | Sum-modified-Laplacian

In the transform area, high-frequency subgroups contain sharp information of the images. To intertwine the high-frequency subgroups, the greatest fusion rule which chooses high-frequency subgroups with most extreme utilized. Consequently, the most extreme strategy is delicate to edges and directional features. To beat the issue of artifacts in the fusion methodology, rather than choosing the pixel with a bigger worth Sum-modified-Laplacian (SML) measure is utilized. In Reference 20, it is discovered that for fusion reason, the presentation of SML is superior to other Laplacian methods. Therefore, in view of image clearness, SML center measure is utilized to meld high-frequency coefficients.

However, modified-laplacian (ML) can give remarkable highlights and sharp information on the image. The sum of the encompassing ML is indicated by SML which yields the neighborhood proportions of the nature of the image center. It is observed that SML is more effective than ML in the frequency area, especially for high frequencies. In this manner, SML is utilized to meld the high-frequency coefficients. The meaning of SML is given as :

$$S(m,n) = \sum_{i\prime=m-N}^{i\prime=m+N} \sum_{j\prime=n-N}^{j\prime=n+N} M(i\prime, j\prime), \tag{4}$$

where N determines the block size $(2\times N+1)\times(2\times N+1)$ used to estimate the focus measure. $M(m, n)$, denotes the value of modified Laplacian located at (m, n) can be defined as:

$$M(m,n) = |2I(m,n) - I(m-1,n) - I(m+1,n)| \tag{5}$$
$$+ |2I(m,n) - I(m,n-1) - I(m,n+1)|, \tag{5}$$

where $I(m,n)$ indicates the pixel value at the position (m,n).

3 | PROPOSED METHOD

The objective of the proposed method is to gain more informative images in comparison to input multimodality images. Therefore in the proposed method, the NSST transform is utilized so that multidirectional information of high-frequency subbands of input images can be fused and provide maximum information. To get the maximum information, the fusion approach is utilized on the basis of correlation analysis and the SML method. In proposed method, firstly NSST transform is applied on both input images to get low and high frequencies. In the low-frequency components, correlation-based fusion is performed. Similarly, high-frequency components are fused using SML approach. The detail of our proposed fusion method for multimodality images is discussed below.

Step 1 (Fusion of low-frequency coefficients): The low-frequency coefficients are fused by utilizing the correlation-based fusion approach. Here, patch wise correlation values between both input images are obtained.

$$CC = \frac{\sum_{i=1}^{m}\sum_{j=1}^{n}(A_{XX} - \overline{A_{XX}}) \cdot (A_{YY} - \overline{A_{YY}})}{\sqrt{\sum_{i=1}^{m}\sum_{j=1}^{n}(A_{XX} - \overline{A_{XX}})^2 \cdot \sum_{i=1}^{m}\sum_{j=1}^{n}(A_{YY} - \overline{A_{YY}})^2}}, \tag{6}$$

where $A_{XX} = A_{l,p}^{X}(i,j)$ and $A_{YY} = A_{l,p}^{Y}(i,j)$.

$\overline{A_{XX}} = \text{mean}(A_{l,p}^{X}(i,j))$ and $\overline{A_{YY}} = \text{mean}(A_{l,p}^{Y}(i,j))$ represent mean of their respective low-frequency components.

In correlation-based fusion procedure, acquired correlation esteem (CC) is contrasted and the limit esteem (T). Here in this work, the limit esteem T is gotten by computing normal of nearby correlation esteems and worldwide correlation esteems. On the off chance that the estimation of correlation coefficients is not exactly or equivalent to the edge esteem, at that point most extreme technique is performed. In most extreme strategies, fusion is performed by choosing the biggest qualities from both of the changed images. Generally, the averaging technique is utilized, which figures the normal worth

utilizing both the changed images to perform the fusion. Correlation-based fusion methodology is given as follows:

$$\mathrm{NSST}_L(\mathrm{new}) = \begin{cases} \max(\mathrm{NSST}_{\mathrm{Low}(A)}, \mathrm{NSST}_{\mathrm{Low}}(B)), & if \quad (\mathrm{CC} \leq T) \\ \mathrm{avg}(\mathrm{NSST}_{\mathrm{Low}}(A), \mathrm{NSST}_{\mathrm{Low}}(B)), & \text{otherwise} \end{cases} \tag{7}$$

Step 2 (Fusion of high-frequency coefficients): The high-frequency NSST coefficients are fused using SML where blockwise SML-based fusion rule is performed. The SML rule is trailed by the greatest strategy and performed over every block. The below equation shows the fusion operation which is performed over the NSST high-frequency coefficients.

$$\mathrm{NSST}_H(new) = \begin{cases} \mathrm{NSST}_{\mathrm{High}}(A), & if : \mathrm{SML}_{\mathrm{NSST}_{High}(A)} \geq \mathrm{SML}_{\mathrm{NSST}_{\mathrm{High}}(B)} \\ \mathrm{NSST}_{\mathrm{High}}(B), & \text{otherwise} \end{cases}, \tag{8}$$

where, $\mathrm{SML}_{\mathrm{NSST}_{\mathrm{High}}(A)}and\mathrm{SML}_{\mathrm{NSST}_{\mathrm{High}}(B)}$ are the coefficients which are obtained by SML method.

Step 3 (Intermediate Reconstructed fused image): The final reconstructed fused image is achieved by performing inverse NSST over the fused coefficients.

Step 4 (Method noise thresholding): In this step, the fused image which is obtained from step 3 is subtracted from both input images. Over both subtracted images, NSST based thresholding is performed using below thresholding function. The detail of this thresholding function is given in Reference 19:

$$\theta(y_k) = \begin{cases} 0, & if \quad \theta(y_k) < 0 \\ \theta(y_k), & \text{otherwise} \end{cases}, \tag{9}$$

where $\theta(y_k) = \sum_{s=1}^{2} a_s \varphi_s(y_k)$.

Step 5: The outcome of step 4 is both denoised subtracted images are fused using Steps 1 to 3.

Step 6: To get the final fused image, both results of Step 3 and Step 5 are added.

For encryption and decryption over the fused image, a pseudorandom number framework[17] Z is developed by pseudorandom-number generator (PRNG) with the help of an encryption key. Further, the encryption process is performed by expansion modulo 256 to get the encoded image P as follows :

$$P(p,q) = (A(p,q) + Z(p,q)) \ mod \ 256. \tag{10}$$

Here, Z are pseudorandom numbers and A is a fused image.

Encoded combined image P is decoded utilizing following unscrambling system. For decoding P, pseudorandom numbers framework Z is produced utilizing encryption key and afterward the image P is unscrambled to get the straightforwardly decoded combined image P' utilizing underneath condition.

$$P'(i,j) = (P(i,j) - Z(i,j)) \ mod \ 256. \tag{11}$$

4 | RESULTS AND DISCUSSIONS:

4.1 | Source images

To obtain and examine the results of the proposed method, the multimodality image dataset is obtained via[15] as shown in Figures 1 to 7. The resolution of all source images is 256×256. The results are tested over the 80 image pair of CT-MRI, MRI-SPECT, and other medical image pairs.

4.2 | Method of comparison

To examine the performance of the proposed method, various standard similar methods are used to show the capability of the proposed method. Here, seven NSST-based methods are used for the comparison such as NSST,[2] NSST,[7] NSST,[12] NSST,[29] NSST,[20] NSST,[28] and NSST.[31] For a fair comparison, the decomposition level of all methods is the same which is 4.

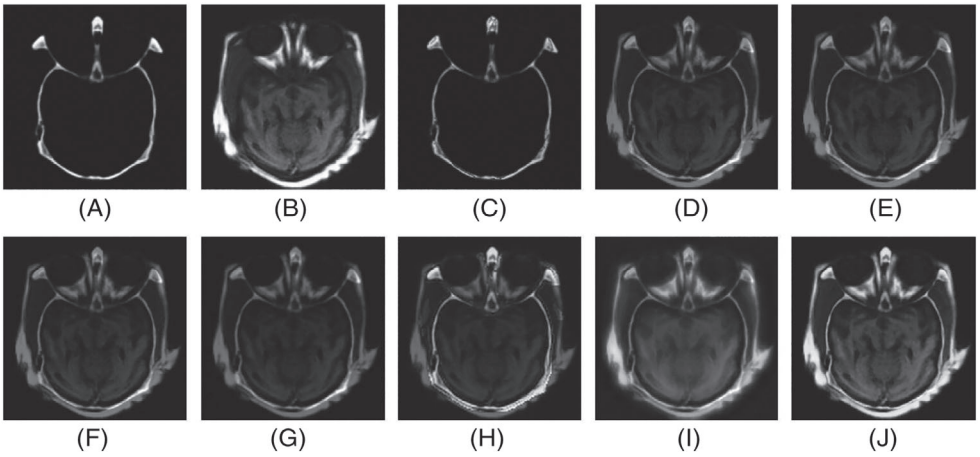

FIGURE 1 (A) and (B) are input multimodality medical images, (C) Result of Reference 2, (D) Result of Reference 7, (E) Result of Reference 12, (F) Result of Reference 29, (G) Result of Reference 20, (H) Result of Reference 28, (I) Result of Reference 31, (J) Proposed method

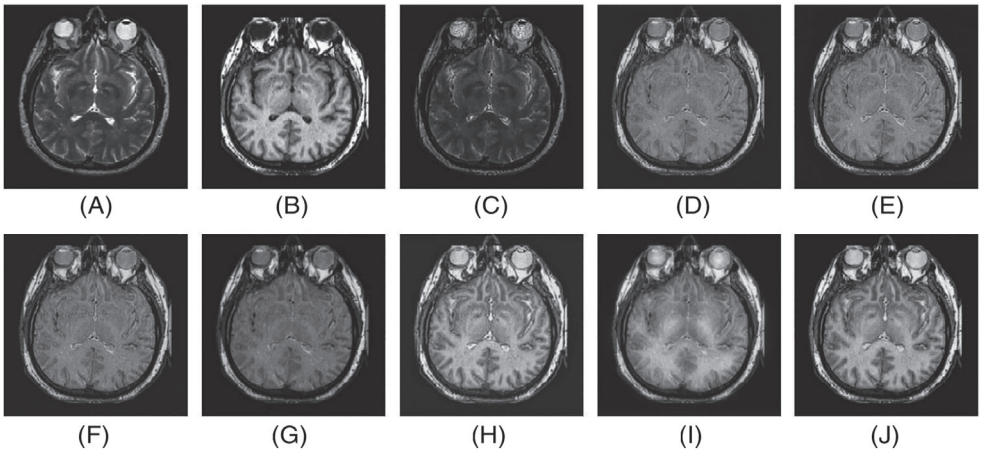

FIGURE 2 (A) and (B) are input multimodality medical images, (C) Result of Reference 2, (D) Result of Reference 7, (E) Result of Reference 12, (F) Result of Reference 29, (G) Result of Reference 20, (H) Result of Reference 28, (I) Result of Reference 31, and (J) Proposed method

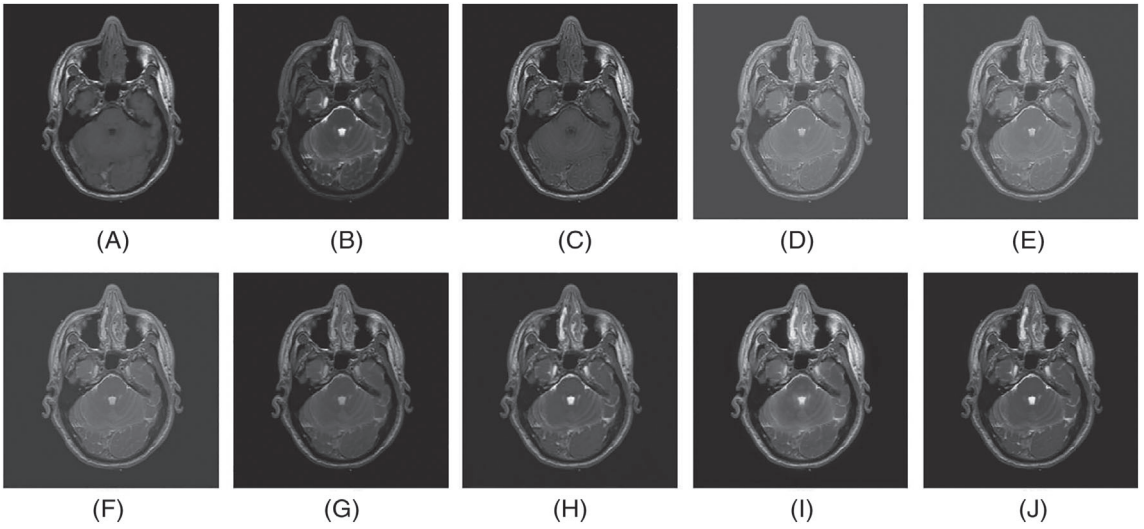

FIGURE 3 (A) and (B) are input multimodality medical images; (C) Result of Reference 2, (D) Result of Reference 7, (E) Result of Reference 12, (F) Result of Reference 29, (G) Result of Reference 20, (H) Result of Reference 28, (I) Result of Reference 31, (J) Proposed method

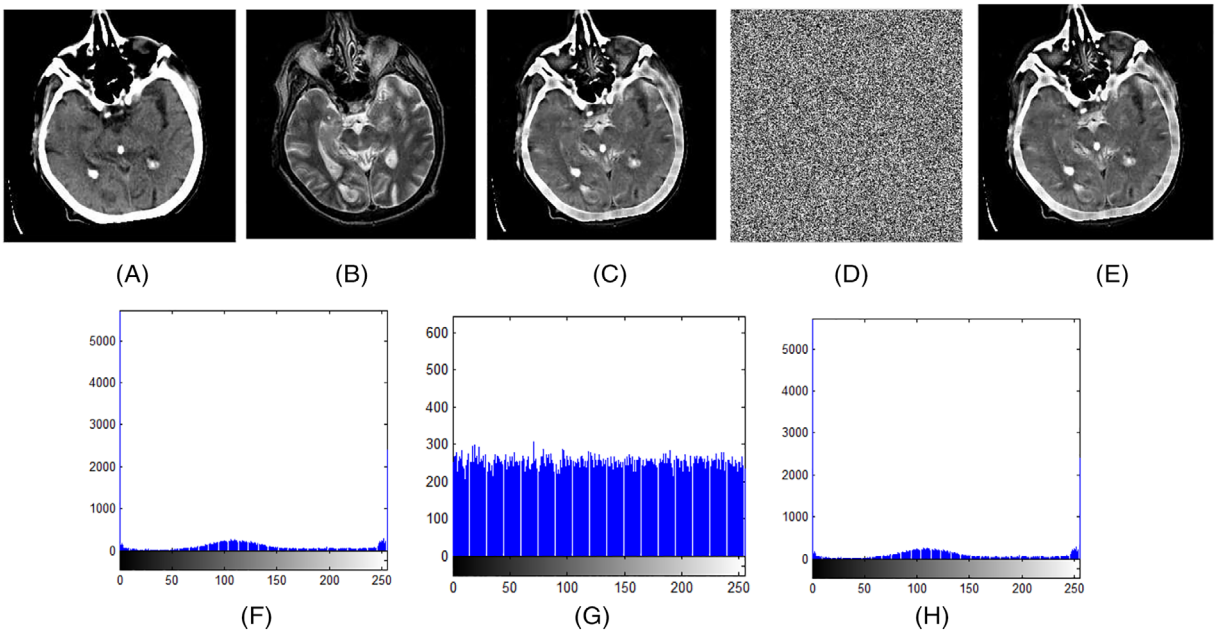

FIGURE 4 (A) and (B) are input multimodality medical images, (C) Result of Proposed method, (D) Encrypted image over the result of proposed method, (E) Decrypted image, (F) Histogram of (C), (G) Histogram of (D), (H) Histogram on (E)

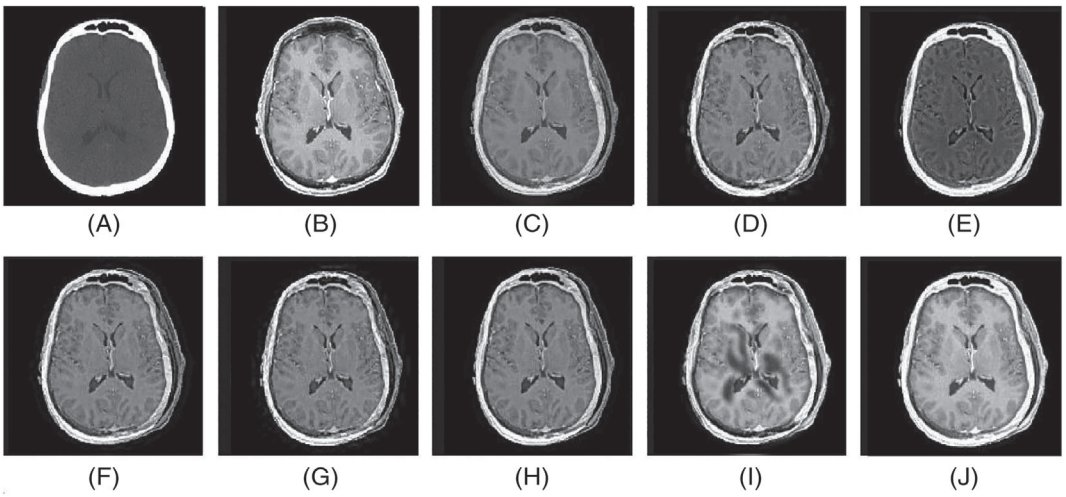

FIGURE 5 (A) and (B) are input multimodality medical images, (C) Decrypted image over the Result of Reference 2, (D) Decrypted image over the Result of Reference 7, (E) Decrypted image over the Result of Reference 12, (F) Decrypted image over the Result of Reference 29, (G) Decrypted image over the Result of Reference 20, (H) Decrypted image over the Result of Reference 28, (I) Decrypted image over the Result of Reference 31 and (J) Decrypted image over the proposed method

4.3 | Objective Evaluation Metrics

Human eyes are not capable to analyze the minor visual details of the results. Therefore, only visual result analysis is not sufficient to measure the accuracy of the results. Some statistical methods are required to measure the performance of results. Hence, some popular performance metrics are required to analyze the performance of the proposed method in comparison to existing methods. Here performance metrics[15] are used such as correlation ratio (CC), SD, Entropy (En), average gradient (AG), Average Pixel Intensity (API), mutual information (MI), Fusion Symmetry (FS), Spatial Frequency (SF), Petrovic Metric Parameter Q_{ABF}, Petrovic Metric Parameter L_{ABF}, and Petrovic Metric Parameter N_{ABF}. The higher value of all mentioned performance metrics gives the best results. Some popular performance metrics are defined below:

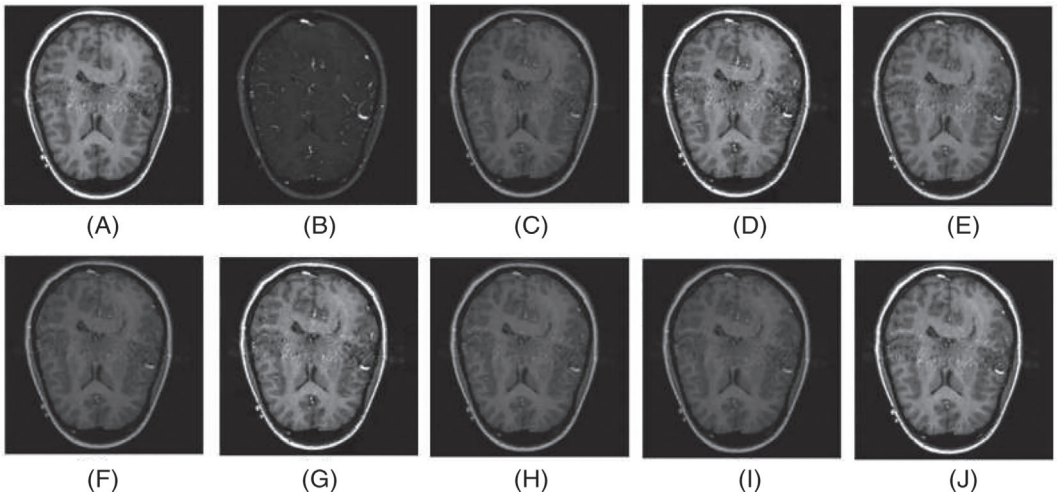

FIGURE 6 (A) and (B) are input multimodality medical images, (C) Decrypted image over the Result of Reference 2, (D) Decrypted image over the Result of Reference 7, (E) Decrypted image over the Result of Reference 12, (F) Decrypted image over the Result of Reference 29, (G) Decrypted image over the Result of Reference 20, (H) Decrypted image over the Result of Reference 28, (I) Decrypted image over the Result of Reference 31 and (J) Decrypted image over the proposed method

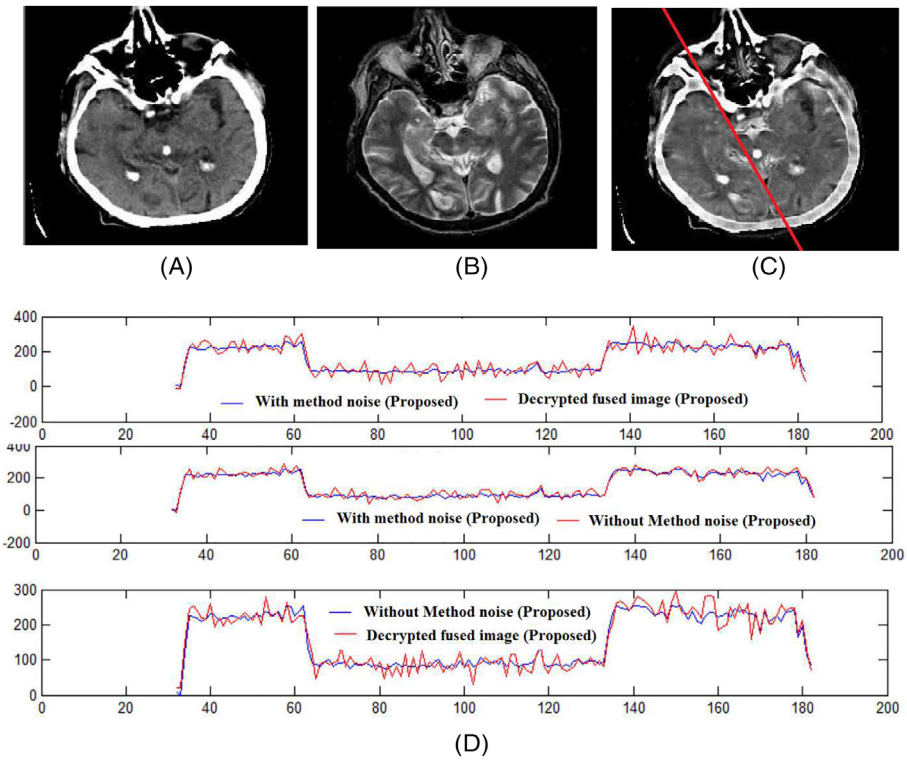

FIGURE 7 (A) and (B) are input multimodality medical images, (C) Result of proposed method, (D) Result of Intensity profile: with method noise, without method noise and over decrypted image using proposed fusion method

4.3.1 | Mean and SD

The mean or average pixel intensity *(API)* and SD is given as:

$$\hat{\mu} = \frac{1}{pq} \sum_{m=1}^{p} \sum_{n=1}^{q} A_{\mathrm{f}}(m, n), \tag{12}$$

$$\mathrm{SD} = \sqrt{\frac{1}{pq-1}\sum_{m=1}^{p}\sum_{n=1}^{q}(A_{\mathrm{f}}(m,n)-\hat{\mu})^2}, \tag{13}$$

where $\hat{\mu}$, SD, and A_{f} represent mean, standard deviation, and fused image, respectively. The SD criterion evaluates the contrast in an image and denotes the discrete image grayscale relative to the mean gray value. If the value of SD is high then the image gray level distribution of dispersion, image contrast is high which provides more information. Hence, the higher value of the SD denotes the high contrast image.

4.3.2 | Edge-based similarity metric ($Q^{AB/I_{\mathrm{f}}}$)

$Q^{AB/I_{\mathrm{f}}}$[16] metric evaluates the amount of edge information transferred from source images (A,B) images to fused image (I_{f}). It is calculated as:

$$Q^{AB/I_{\mathrm{f}}} = \frac{\sum_{p=1}^{m}\sum_{q=1}^{n}(Q^{AI_{\mathrm{f}}}(p,q).w^{A}(p,q) + Q^{BI_{\mathrm{f}}}(p,q).w^{B}(p,q))}{\sum_{p=1}^{m}\sum_{q=1}^{n}(w^{A}(p,q)+w^{B}(p,q))}, \tag{14}$$

where $w^A(p,q)$ and $w^B(p,q)$ denote the weight for edge preservation values $Q^{AI_{\mathrm{f}}}$ and $Q^{BI_{\mathrm{f}}}$, respectively. The definitions of $Q^{AI_{\mathrm{f}}}$ and $Q^{BI_{\mathrm{f}}}$ are same and given as:

$$Q^{AI_{\mathrm{f}}}(p,q) = Q_g^{AI_{\mathrm{f}}}(p,q).Q_\alpha^{AI_{\mathrm{f}}}(p,q), \tag{15}$$

where $Q_g^{AI_{\mathrm{f}}}(p,q)$ and $Q_\alpha^{AI_{\mathrm{f}}}(p,q)$ represent the edge strength and orientation values at location p and q, respectively. The metrics $L^{AB/I_{\mathrm{f}}}$, $N^{AB/I_{\mathrm{f}}}$, and $N_m^{AB/I_{\mathrm{f}}}$ are used to compute the total loss of information and noise or artifacts in fused image which are given in Reference 16.

4.3.3 | Average gradient

It define the smoothness and sharpness, as:

$$AG = \frac{\sum_{p=1}^{m}\sum_{q=1}^{n}((I_{\mathrm{f}}(p,q)-I_{\mathrm{f}}(p+1,q))^2 + (I_{\mathrm{f}}(p,q)-I_f(p,q+1))^2))^{1/2}}{mn}. \tag{16}$$

4.3.4 | Entropy

It is used to measure the quality of images using average amount of information, as:

$$\mathrm{EN} = -\sum_{k=0}^{255} p_k \lg_2(p_k), \tag{17}$$

where p_k is the probability of intensity value k in image.

4.3.5 | Mutual Information

It is used to measure the quality of images using total amount of information, as given below:

$$I_{A,I_f} = \sum_{p,q} h_{A,I_f}(p,q) \log \frac{h_{A,I_f}(p,q)}{h_A(p) h_{I_f}(q)}, \tag{18}$$

where h_{A,I_f} is the jointly normalized histogram; h_A and h_{I_f} are normalized histogram of AandI_{f}, respectively. Similarly, I_{B,I_f} represents the mutual information between other source image Bandfused image I_f. Hence, the total (MI) between the source images A,B and fused image I_f is given as:

$$\mathrm{MI} = I_{A,I_f} + I_{B,I_f}. \tag{19}$$

4.4 | Comparative result analysis

The results are evaluated via two categories: visually and performance metrics. Visuality the images are analyzed in terms of features such as edges, contrast, artifacts, texture, homogenous regions, and so on. However, our naked eyes are not so capable to see the very minor differences between resultant images to compare the results of existing methods. Therefore, the performance metrics role comes to find the best results.

Here some visual results are shown such as in Figures 1-7. In Figure 1, the first two images are the input images and others are the results of fusion methods. here, visually can be analyzed that the results of the proposed scheme get maximum information in comparison to existing results. However, the visual results indicate that some details such as edges and bone details are better shown in the proposed method results. However, Figure 1H showing the higher contrast and due that edges are not so clearly recognized. In Figure 2, the first two images are input images and others are the results of the fusion methods. In Figure 2C,D, the edges are not so clear and texture is missing. However, Figures 2E to G,I, give better edges but the texture is not accurately preserved. In Figure 2H,J both have good quality results and visually both contain better features such as edges and textures. The results are also evaluated over new images as shown in Figure 3. The first two images are input images and others are results of fusion methods. Figure 3D to F contains high contrast which affects the quality of the image details. However, the result of the proposed method as shown in Figure 3H gives better outcomes in terms of edges, textures, and contrast. The results are also tested through performance metrics as shown in Table 1. In Table 1, the average values are shown which is tested over the five multimodality pair of the test images as shown in Figures 1 to 5. After estimating performance metrics, it was observed that most of the time the results of the proposed method are better. Here from Table 1 which contains average values, it can be analyzed that the results of the proposed method are better.

TABLE 1 Image fusion performance measure: Average results over the Dataset 1 to 5

Input images	Fusion rules	SD	CC	API	AG	EN	MI	FS	SF	$Q^{XY/f}$	$L^{XY/f}$	$N^{XY/f}$	$N_m^{XY/f}$
	[2]	85.145	0.9721	97.081	3.879	3.8869	5.728	1.8904	6.2841	0.8341	0.1659	0.0017	0.0016
	[7]	85.125	0.9754	97.031	3.878	4.3445	5.875	1.8722	6.2817	0.8338	0.1662	0.0021	0.0013
Dataaet (1 to 5)	[12]	83.082	0.9872	97.118	4.471	4.4882	6.492	1.9021	7.4981	0.8700	0.1299	0.0118	0.0010
	[29]	85.921	0.9869	96.811	5.1265	7.1115	7.1025	1.9606	8.6122	0.8232	0.0951	0.0131	0.0014
	[20]	86.242	0.9809	96.418	4.4225	6.2755	6.1325	1.9140	8.4522	0.8921	0.0987	0.0113	0.0021
	[28]	86.322	0.9823	96.141	4.6125	6.4445	6.4325	1.9650	8.2322	0.8976	0.0985	0.0176	0.0019
	[31]	86.845	0.9909	96.584	5.5511	7.2114	7.3112	1.9430	8.4122	0.8987	0.0991	0.0134	0.0023
	Proposed	87.417	0.9931	98.899	6.8644	7.9561	7.8667	1.9934	9.5015	0.8983	0.2475	0.0515	0.0033

Abbreviations: CC, correlation ratio; En, Entropy; AG, average gradient; API, Average Pixel Intensity; MI, mutual information; FS, Fusion Symmetry; SF, Spatial Frequency.

Further these fused images are transmitted in a secure domain. Hence, the encryption technique is applied using the PRNG concept as discussed in the proposed methodology. Figure 4 showing the results of the proposed method over the secure domain. The first two images in Figure 4 showing the input image and fusion are performed via the proposed method which is shown in Figure 4C. This fused image is encrypted using the PRNG method and a fused encrypted image is obtained as shown in figure 4(d). This encrypted fused image is decrypted as discussed in the proposed methodology and the decrypted image is obtained as shown in Figure 4E. To measure the security issues, the histogram analysis is performed as shown in Figure 4F to H. In comparison to Figure 4F,H, it is observed that the image is decrypted correctly. Figures 5 and 6 are showing the results of decrypted fused images. Figure 5A,B are the input images and Figures 5C to J are the results of decrypted images of fused images using fusion methods. Similarly Figure 6A,B are the input images and Figure 6C to J are the results of decrypted images of fused images using fusion methods. Here, the results of decrypted fused images are also indicating that the outcomes of proposed method contain better features in comparison to existing methods.

In the proposed methodology, the method noise thresholding concept is used. to show the effectiveness of method noise thresholding, some results are evaluated between with-method noise, without method noise in proposed methodology and also between decrypted fused images. These comparative results are shown in Table 2. Table 2 contains the average results of dataset 1 to 5 which are shown in Figures 1 to 5. From Table 2, it is analyzed that with method noise proposed methodology gives better outcomes in compare to without method noise. It can also be analyzed that decrypted fused images using the proposed methodology (with method noise) gives better outcomes in comparison to without method noise (proposed methodology). This shows the effectiveness of method noise thresholding in the proposed methodology. The effectiveness of proposed methodology can also be analyzed by the intensity profile results as shown in Figure 7. First two images are input images as shown in Figures 7A,B and Figure 7C is fused image using proposed methodology (with method noise). Figure 7D indicating the intensity profile between with method noise (proposed method), without method noise (proposed method) and decrypted fused images (proposed method). However, the results of proposed method may vary as the parameters values are changed such as decomposition levels. However, this difficulty can be resolved by finding optimum decomposition level by obtaining results from different decomposition levels.

To measure the computational burden issue, the execution time is estimated for proposed method as well as for existing methods. The execution time is evaluated over the 80 pair medical images. Finally, the average execution time of methods (proposed and existing) is estimated which is shown in Table 3. From Table 3, it can be clearly analyzed that proposed methodology has less computation time in compare to existing. However, other existing methods have close results in terms of execution time. However, there is a tradeoff between performance of methods and execution time. But here it can be concluded that in most cases both execution time and performance of the proposed method is up to the mark.

TABLE 2 A comparative result analysis between with method noise, without method noise and decrypted fused images: An average result from dataset 1 to 5

Indices	Decrypted Fused image (Proposed))	Proposed Method (Without Method Noise)	Proposed Method (With Method Noise)
Mean	119.1268	119.1555	119.5538
SD	50.8325	51.1246	51.2989
CC	0.9643	0.9847	0.9889
Entropy	34.2197	34.5824	34.9147
MI	7.0117	7.4521	7.8412
AG	6.82315	7.4126	7.9127

Abbreviations: AG, average gradient; CC, correlation ratio; MI, mutual information; MI, mutual information.

TABLE 3 Average computation time (in seconds) over 80 pair multimodality images

Method	2	7	12	29	20	28	31	Proposed
Time	2.1221	1.1512	2.2275	1.6127	0.9667	0.9831	1.3342	0.9145

5 | CONCLUSIONS

In this paper, a new fusion method is given using the approach of method noise thresholding which is also tested in an encrypted environment. The effectiveness of the proposed methodology is also tested without a method noise thresholding concept where it is clearly indicated that the proposed methodology using the approach of method noise thresholding gives better outcomes in comparison to existing and also without method noise thresholding in the proposed methodology. The visual results are tested which also indicates that the proposed method gives good quality of fused images in comparison to existing methods. The overall performance metrics also showed that the proposed method gives better outcomes. for more critical analysis of proposed method, intensity profile is also tested which also indicates the for better outcomes. Hence, it can be concluded that the method noise thresholding improves the results of the fused images effectively. It is also confirmed from the result analysis that in most cases the proposed method gives better outcomes in comparison to existing over the secure (encrypted) environment.

ORCID

Manoj Diwakar https://orcid.org/0000-0002-4435-675X

REFERENCES

1. Burute N, Jankharia B. Teleradiology: the Indian perspective. *Indian J Radiol Imaging*. 2009;19(1):16.
2. Wang L, Li B, Tian LF. Multi-modal medical image fusion using the inter-scale and intra-scale dependencies between image shift-invariant shearlet coefficients. *Inf Fusion*. 2014;19:20-28.
3. Vu DL, Nguyen TK, Nguyen TV, Nguyen TN, Massacci F, Phung PH. HIT4Mal: hybrid image transformation for malware classification. *Trans Emerg Telecommun Technol*. 2019;e3789.
4. Khare P, Srivastava VK. A secured and robust medical image watermarking approach for protecting integrity of medical images. *Trans Emerg Telecommun Technol*. 2020.
5. Lydia EL, Raj JS, Pandi Selvam R, Elhoseny M, Shankar K. Application of discrete transforms with selective coefficients for blind image watermarking. *Trans Emerg Telecommun Technol*. 2019;e3771.
6. Hassan H, Bashir AK, Abbasi R, Ahmad W, Luo B. Single image defocus estimation by modified Gaussian function. *Trans Emerg Telecommun Technol*. 2019;30(6):e3611.
7. Singh S, Gupta D, Anand RS, Kumar V. Nonsubsampled shearlet based CT and MR medical image fusion using biologically inspired spiking neural network. *Biomed Signal Process Control*. 2015;18:91-101.
8. Liu X, Mei W, Du H, Bei J. A novel image fusion algorithm based on nonsubsampled shearlet transform and morphological component analysis. *Signal Image Video Process*. 2016;10(5):959-966.
9. Ganasala P, Kumar V. Multimodality medical image fusion based on new features in NSST domain. *Biomed Eng Lett*. 2014;4(4):414-424.
10. Luo X, Zhang Z, Zhang B, Wu X. Image fusion with contextual statistical similarity and nonsubsampled shearlet transform. *IEEE Sens J*. 2016;17(6):1760-1771.
11. Kong W, Liu J. Technique for image fusion based on nonsubsampled shearlet transform and improved pulse-coupled neural network. *Opt Eng*. 2013;52(1):017001.
12. Ganasala P, Kumar V. Feature-motivated simplified adaptive PCNN-based medical image fusion algorithm in NSST domain. *J Dig Imaging*. 2016;29(1):73-85.
13. Liu X, Mei W, Du H. Structure tensor and nonsubsampled shearlet transform based algorithm for CT and MRI image fusion. *Neurocomputing*. 2017;235:131-139.
14. http//www.med.harvard.edu/AANLIB/. Accessed 2 2015.
15. Piella G, Heijmans H. A new quality metric for image fusion. Paper presented at: Proceedings of the 2003 International Conference on Image Processing (Cat. No. 03CH37429); September, Vol. 3, 2003:III-173; IEEE.
16. Qu G, Zhang D, Yan P. Information measure for performance of image fusion. *Electron Lett*. 2002;38(7):313-315.
17. Lakshmi VS, Deepthi PP. An efficient scheme for secure domain medical image fusion over cloud. *Multimedia Tools Appl*. 2019;78(15):20609-20636.
18. Ramlal SD, Sachdeva J, Ahuja CK, Khandelwal N. An improved multimodal medical image fusion scheme based on hybrid combination of nonsubsampled contourlet transform and stationary wavelet transform. *Int J Imaging Syst Tech*. 2019;29(2):146-160.
19. Diwakar M, Singh P. CT image denoising using multivariate model and its method noise thresholding in non-subsampled shearlet domain. *Biomed Signal Process Control*. 2020;57:101754.
20. Ullah H, Ullah B, Wu L, Abdalla FY, Ren G, Zhao Y. Multi-modality medical images fusion based on local-features fuzzy sets and novel sum-modified-Laplacian in non-subsampled shearlet transform domain. *Biomed Signal Process Control*. 2020;57:101724.
21. Polinati S, Dhuli R. Multimodal medical image fusion using empirical wavelet decomposition and local energy maxima. *Optik*. 2020;205:163947.
22. Sahu S, Singh HV, Kumar B, Singh AK, Kumar P. Image processing based automated glaucoma detection techniques and role of de-noising: a technical survey. *Handbook of Multimedia Information Security: Techniques and Applications*. Switzerland : Springer; ; 2019:359-375.

23. Sahu S, Singh HV, Kumar B, Singh AK, Kumar P. Enhancement and de-noising of OCT image by adaptive wavelet thresholding method. *Handbook of Multimedia Information Security: Techniques and Applications*. Switzerland : Springer; 2019;449-471.
24. Moonon AU, Hu J, Li S. Remote sensing image fusion method based on nonsubsampled shearlet transform and sparse representation. *Sens Imaging*. 2015;16(1):23.
25. Diwakar M, Kumar P, Singh AK. CT image denoising using NLM and its method noise thresholding. *Multimedia Tools Appl*. 2018;1-16.
26. Sahu S, Singh HV, Kumar B, Singh AK. Statistical modeling and Gaussianization procedure based de-speckling algorithm for retinal OCT images. *J Ambient Intell Humaniz Comput*. 2018;1-14.
27. Sahu S, Singh HV, Kumar B, Singh AK. De-noising of ultrasound image using Bayesian approached heavy-tailed Cauchy distribution. *Multimedia Tools Appl*. 2019;78(4):4089-4106.
28. Gupta D. Nonsubsampled shearlet domain fusion techniques for CT MR neurological images using improved biological inspired neural model. *Biocybernet Biomed Eng*. 2018;38(2):262-274.
29. Yin M, Liu X, Liu Y, Chen X. Medical image fusion with parameter-adaptive pulse coupled neural network in nonsubsampled shearlet transform domain. *IEEE Trans Instrument Measur*. 2018;68(1):49-64.
30. Liu X, Mei W, Du H. Multi-modality medical image fusion based on image decomposition framework and nonsubsampled shearlet transform. *Biomed Signal Process Control*. 2018;40:343-350.
31. Jin X, Chen G, Hou J, Jiang Q, Zhou D, Yao S. Multimodal sensor medical image fusion based on nonsubsampled shearlet transform and S-PCNNs in HSV space. *Signal Process*. 2018;153:379-395.
32. El-Hoseny HM, El-Rahman WA, El-Shafai W, et al. Efficient multi-scale non-sub-sampled shearlet fusion system based on modified central force optimization and contrast enhancement. *Infrared Phys Tech*. 2019;102:102975.
33. Tang L, Qian J, Li L, Hu J, Wu X. Multimodal medical image fusion based on discrete Tchebichef moments and pulse coupled neural network. *Int J Imag Syst Tech*. 2017;27:57-65.
34. Bhatnagar G, Wu QJ, Liu Z. A new contrast based multimodal medical image fusion framework. *Neurocomputing*. 2015;157:143-152.
35. Ramlal SD, Sachdeva J, Ahuja CK, Khandelwal N. Multimodal medical image fusion using non-subsampled shearlet transform and pulse coupled neural network incorporated with morphological gradient. *Signal Image Video Process*. 2018;12:1479-1487.
36. Gomathi PS, Kalaavathi B. Multimodal medical image fusion in nonsubsampled contourlet transform domain. *Circ Syst*. 2016;7:1598-1610.
37. Yang L, Guo B, Ni W. Multimodality medical image fusion based on multiscale geometric analysis of contourlet transform. *Neurocomputing*. 2008;72:203-211.
38. Jiang W, Yang X, Wu W, et al. Medical images fusion by using weighted least squares filter and sparse representation. *Comput Electr Eng*. 2018;67:252-266.
39. Ramlal SD, Sachdeva J, Ahuja CK, Khandelwal N. Brain CT and MR image fusion framework based on stationary wavelet transform. In: Bhatia S, Mishra K, Tiwari S, Singh V, eds. *Advances in Computer and Computational Sciences. Advances in Intelligent Systems and Computing*. Vol 554. Singapore: Springer; 2018:445-453.

How to cite this article: Kumar P, Diwakar M. A novel approach for multimodality medical image fusion over secure environment. *Trans Emerging Tel Tech*. 2020;e3985. https://doi.org/10.1002/ett.3985